

RESEARCH ARTICLE

Open Access



# Changes in hip joint contact stress during a gait cycle based on the individualized modeling method of “gait-musculoskeletal system-finite element”

Binglang Xiong<sup>1,2,3</sup>, Peng Yang<sup>1,2,3,7</sup>, Tianye Lin<sup>1,2,3</sup>, Jingli Xu<sup>1,2,3</sup>, Yong Xie<sup>4</sup>, Yongliang Guo<sup>5</sup>, Churong Liu<sup>5</sup>, Qizhao Zhou<sup>1,2,3</sup>, Qizhong Lai<sup>1,2,3</sup>, Wei He<sup>6\*</sup>, Qiushi Wei<sup>6\*</sup> and Qingwen Zhang<sup>6\*</sup> 

## Abstract

**Objective:** To construct a comprehensive simulation method of “gait-musculoskeletal system (MS)-finite element (FE)” for analysis of hip joint dynamics characteristics and the changes in the contact stress in the hip throughout a gait cycle.

**Methods:** Two healthy volunteers (male and female) were recruited. The 3D gait trajectories during normal walking and the CT images including the hip and femur of the volunteers were obtained. CT imaging data in the DICOM format were extracted for subjected 3D hip joint reconstruction. The reconstructed 3D model files were used to realize the subject-specific registration of the pelvis and thigh segment of general musculoskeletal model. The captured marker trajectory data were used to drive subject-specific musculoskeletal model to complete inverse dynamic analysis. Results of inverse dynamic analysis were exported and applied as boundary and load settings of the hip joint finite element in ABAQUS. Finally, the finite element analysis (FEA) was performed to analyze contact stress of hip joint during a gait cycle of left foot.

**Results:** In the inverse dynamic analysis, the dynamic changes of the main hip-femoral muscle force with respect to each phase of a single gait cycle were plotted. The hip joint reaction force reached a maximum value of 2.9%BW (body weight) and appeared at the end of the terminal stance phase. Twin peaks appeared at the initial contact phase and the end of the terminal stance phase, respectively. FEA showed the temporal changes in contact stress in the acetabulum. In the visual stress cloud chart, the acetabular contact stress was mainly distributed in the dome of the acetabulum and in the anterolateral area at the top of the femoral head during a single gait cycle. The acetabular contact area was between 293.8 and 998.4 mm<sup>2</sup>, and the maximum contact area appear at the mid-stance phase or the loading response phase of gait. The maximum contact stress of the acetabulum reached 6.91 MPa for the model 1 and 6.92 MPa for the model 2 at the terminal stance phase.

**Conclusions:** The “Gait-MS-FE” technology is integrated to construct a comprehensive simulation framework. Based on human gait trajectories and their CT images, individualized simulation modeling can be achieved. Subject-specific

\*Correspondence: hewei141456@163.com; weiqiushi0092@163.com; zhangqingwen1121@163.com

<sup>6</sup>The Third Affiliated Hospital, Guangzhou University of Chinese Medicine, Guangzhou 510240, Guangdong, China  
Full list of author information is available at the end of the article

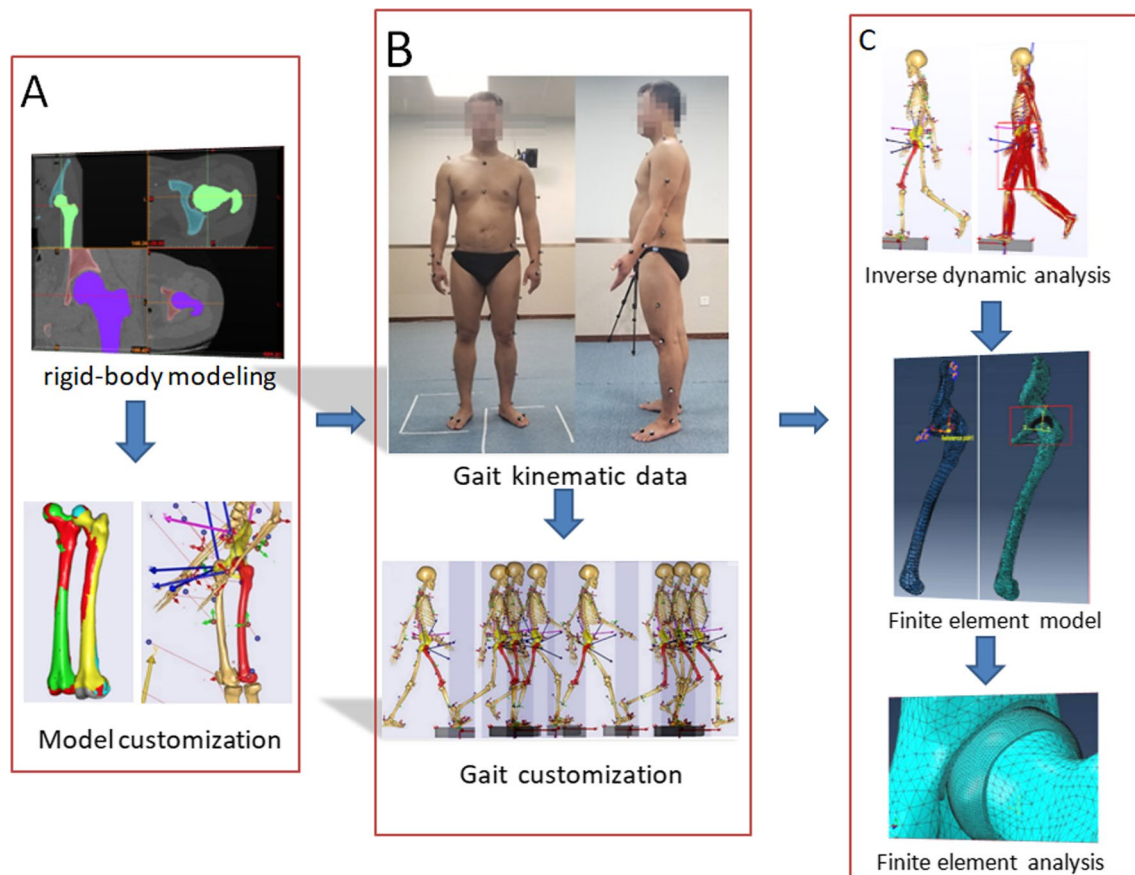


© The Author(s) 2022. **Open Access** This article is licensed under a Creative Commons Attribution 4.0 International License, which permits use, sharing, adaptation, distribution and reproduction in any medium or format, as long as you give appropriate credit to the original author(s) and the source, provide a link to the Creative Commons licence, and indicate if changes were made. The images or other third party material in this article are included in the article's Creative Commons licence, unless indicated otherwise in a credit line to the material. If material is not included in the article's Creative Commons licence and your intended use is not permitted by statutory regulation or exceeds the permitted use, you will need to obtain permission directly from the copyright holder. To view a copy of this licence, visit <http://creativecommons.org/licenses/by/4.0/>. The Creative Commons Public Domain Dedication waiver (<http://creativecommons.org/publicdomain/zero/1.0/>) applies to the data made available in this article, unless otherwise stated in a credit line to the data.

gait in combination with an inverse dynamic analysis of the MS provides pre-processing parameters for FE simulation for more accurate biomechanical analysis of hip joint.

**Keywords:** Gait, Musculoskeletal system, Finite element analysis, Hip biomechanics

### Graphical abstract



### Introduction

Hip arthritis as one of the most common hip diseases is projected to affect 411,000 people in the USA by 2030 [1]. Without appropriate treatment for long time, it will affect daily walking due to a chronic pain in the knee, the spine and other symptoms [2, 3]. Eventually, 572,000 patients could undergo the cost-consuming hip replacement surgery annually until the year 2030 [4, 5]. Therefore, studies about hip joint biomechanics to better understand the occurrence and development of hip diseases have significant clinical and economic implications. In order to simplify the calculation, many biomechanical studies on the hip joint only analyzed the bone model and only considered the effect of the joint force or gravity on the contact stress of the hip joint [6, 7]. To achieve more accurate hip biomechanical analysis,

it is a high priority to consider integrated forces from skeletal structures, as well as surrounding muscles and ligaments of hip joint motion [8]. Moreover, in reality, the hip joint is always in constant motion to complete different activities. In a complete gait cycle, different mechanical states of the hip joint [9] remind us that gait characteristics should also be taken into account for biomechanics studies about the hip joint. However, most of the previous research literature of the finite element (FE) mechanics of the hip joint adopted a simplified model of one-foot standing, and it is believed that the hip bears the greatest force at this time [10–12]. We conducted this research with skepticism and established the “gait-musculoskeletal system (MS)-finite element” hip joint biomechanical research framework to explore the changes in hip joint contact stress during a

gait cycle. Our research method overcomes the shortcomings of previous studies that did not consider muscle strength and gait data.

In previous biomechanical studies [13, 14], the muscle forces around one person's joints obtained in the laboratory were loaded into another person's FE model in the form of loads, while ignoring the differences in individualized muscle forces and the difference in hip joint morphology. These studies did not carry out individualized research. Some studies using the finite element analysis (FEA) have concluded that different pathological morphologies of the hip joint can affect the body-weight loading onto the articular cartilage [15–20]. The shape of the hip joint of standard-sized people is also slightly different. A study by Anderson et al. [21] reported that differences in hip morphology among individuals have a great effect on the contact stress distribution in the hip joint, as much as differences in the gait cycle. The FE model, the loaded muscle force and the gait data used in our study are from the same volunteer, which can truly result in a personalized study of hip joint biomechanics, eliminating the interference of other individual differences.

In this study, the human hip joint was individually simulated using the “gait-MS-FE” method to reconstruct a dynamic hip joint model more accurately. We assumed that the method used in our study was more reasonable than the previous and could achieve personalized biomechanics analysis. We provided a standardized modeling method for subsequent research on hip joint biomechanics. Our purpose was to analyze the changes in the contact stress of the hip joint during a gait cycle. The results obtained can be used to guide clinical decision-making, such as providing reference data for the acetabular rotation angle in hip dysplasia osteotomy. It can also be used for research on daily degeneration of hip joint prosthesis, which is beneficial to the improvement of prosthesis design.

## Methods

### Data collection

A healthy male volunteer (32 years of age, 70 kg, 171 cm) named model 1 and a healthy female volunteer (27 years of age, 51 kg, 162 cm) named model 2 were included in our study. The volunteer didn't have any abnormalities in pelvic posture and hip morphology in pelvic X-ray and CT imaging. The following gait kinematic data of the two volunteers during the current experiment and the follow-up period were obtained. Our study has been approved by the Ethics Committee of the First Affiliated Hospital of Guangzhou University of Chinese Medicine (No. K [2019] 124).

### Imaging data

The region from 1 cm above the highest point of the iliac crest to 3 cm below the trochanter was scanned using X-ray. The images of the pelvis and the femur included three anatomical views of cross section, coronal plane and sagittal plane were obtained by CT (0.5 mm slice thickness, 5 mm wavelength interval, image resolution of  $1024 \times 1024$ , 268 slices for male and 254 slices for female). CT images were saved as DICOM format and exported for 3D rigid-body modeling.

### Gait kinematic data

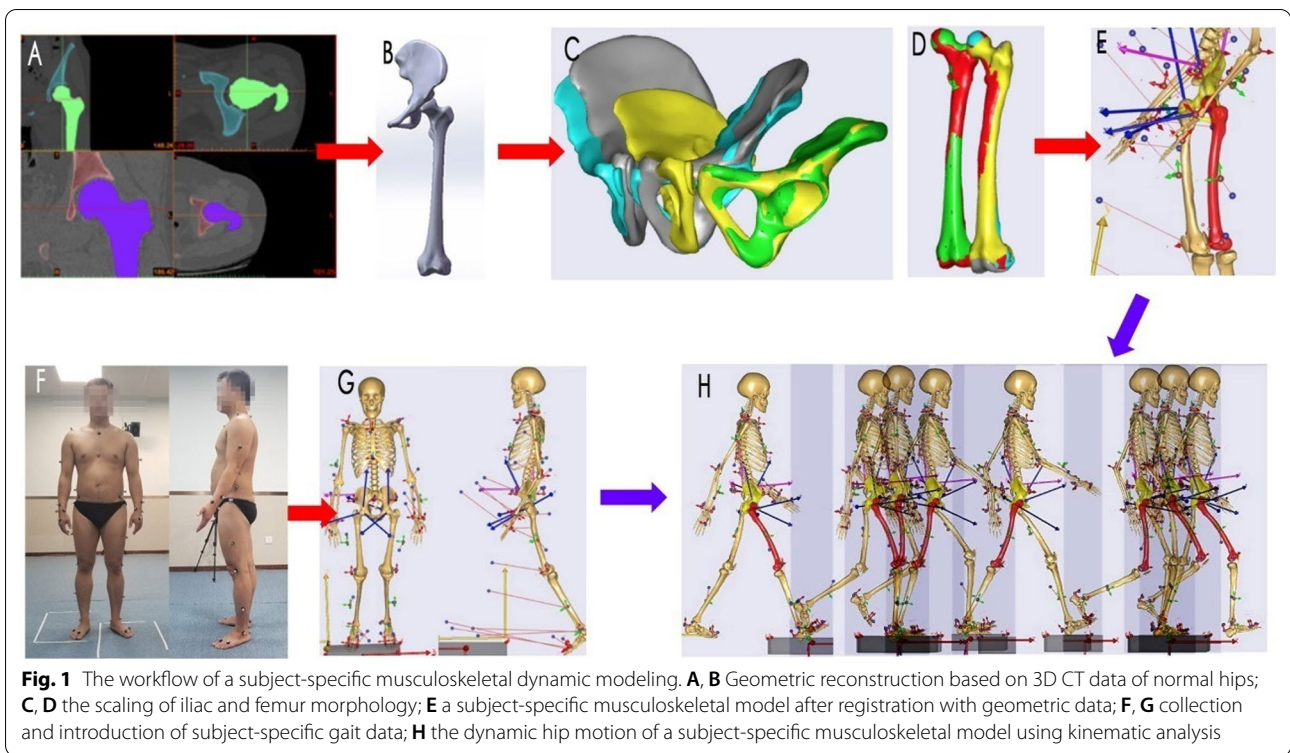
Hip position data of standing posture and gait data of volunteers during walking were collected using the optical 3D gait analysis system (BTS Bioengineering, Italy). During the experiment, the two participants received adaptive training to walk continuously and freely prior to the tests. Then, they underwent 3 rounds of 5-m walk tests to ensure that both feet stepped into the force platform during at least one complete gait cycle in the one-way walking path. Infrared reflective markers were attached to the trunk, arms and legs. Afterwards, gait trajectories were formally collected and saved as the C3D file format for subsequent procedures (Fig. 1F, G).

### Subject-specific musculoskeletal dynamics simulation

The dynamic hip motion of musculoskeletal model was simulated in the AnyBody modeling system (AnyBody Technology Company, Denmark). Custom musculoskeletal dynamics and inverse dynamics were analyzed using a modified full-body model. As the function and application of AnyBody have been reported in similar studies [22], this article focused on the custom simulation process.

### Model customization

To preliminarily adjust scaling of models, the body fat was measured using the built-in formulas in the AnyBody modeling system (volunteers' BMI: model 1: 23.94/model 2: 19.4). To achieve a more accurate self-customization, DICOM data extracted from CT images were used for 3D reconstruction of the ilium and femur using Mimics software (version 16.0, Materialise, Belgium), (Fig. 1A, B). After reconstruction, 3D model files were imported into AnyBody for morphological scaling to determine the subject-specific registration of the pelvis and thigh segment of general musculoskeletal model in AnyBody. That model is based on spatial coordinates of the characteristic points of the iliofemoral models by point-to-point scaling codes. Moreover, the scaling was adjusted to match the starting and ending points of the muscles and ligaments

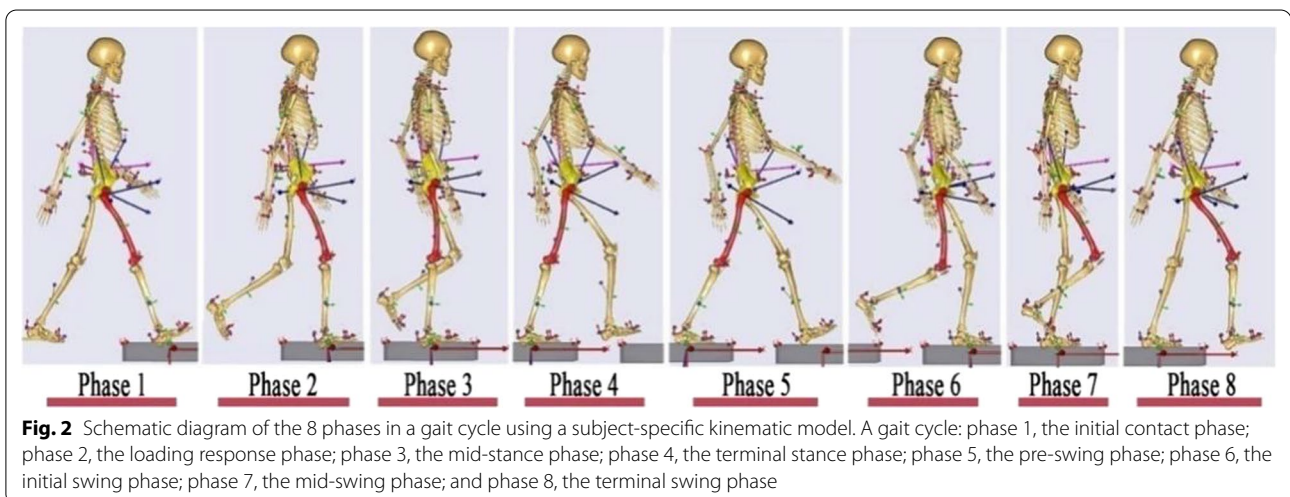


surrounding the hip joint so that the anatomical features of human hip movements could be simulated more accurately (Fig. 1C, D, E).

**Gait customization**

C3D files containing volunteers’ gait data were imported to AnyBody, and the locations of virtual markers alongside their 3D coordinates were adjusted to create the fully matched models in accordance with

the locations of markers attached to the trunk, arms and legs of volunteers. The simulated models were optimized using parameters in the built-in kinematics optimization algorithm in AnyBody, which also simultaneously calculates the movement angles of the hip, ankle joints and the displacement of markers. The dynamic hip motion containing 8 phases in a gait cycle was simulated using the one of optimized multibody model (Fig. 2).



**Inverse dynamic analysis**

Data obtained through kinematics optimization above were re-extracted for inverse dynamics analysis. Muscle importation was solved by formulating a third-order polynomial optimization problem. After the completed corresponding walking gait cycle of the musculoskeletal model during inverse dynamics loading was completed, the data of muscle forces and joint reaction forces of the legs were obtained (Fig. 3). Data of the muscle strength and the kinematics of the hip during a complete gait cycle were extracted for verification.

**FEA for the contact stress distribution**

**Geometric definition**

Subject-specific geometric cartilage model is crucial for biomechanical analysis. Bone morphology has been reported to play an important role to predict cartilage stress [23], and it has also been shown that the optimal alignment of the joint was not sensitive to the choice of cartilage thickness distribution. Therefore, we performed a 3D dilation on the surface of the femoral head and lunate surface of acetabular fossa to reconstruct a

constant thickness (1.8 mm) cartilage layers of the femur and acetabulum [23].

**Material properties and boundary conditions**

As reported in study [24], the cartilage of a normal hip joint was modeled using homogeneous, isotropic and linear elastic materials, while the cortical bone and trabecular of the ilium and femur were modeled using homogeneous isotropic materials (Table 1).

According to the method that has been reported in research [25], data of the 8 phases during a single gait cycle of the left foot were picked to analyze the contact stress of the hip joint during walking using the FEA. In the FE model, rigid transformation parameters of the hip during a gait cycle were adjusted using the kinematic data from the musculoskeletal simulation analysis and obtained by rotating coordinates of all unit nodes of the femur part. Assuming that the original coordinate of the femoral node was  $P(x_0, y_0, z_0)$ , the angles of hip rotation along the three axes of  $x, y$  and  $z$  were  $\theta_x, \theta_y$ , and  $\theta_z$ , and then the three rotation matrices were calculated by Eqs. (1-1), (1-2) and (1-3):

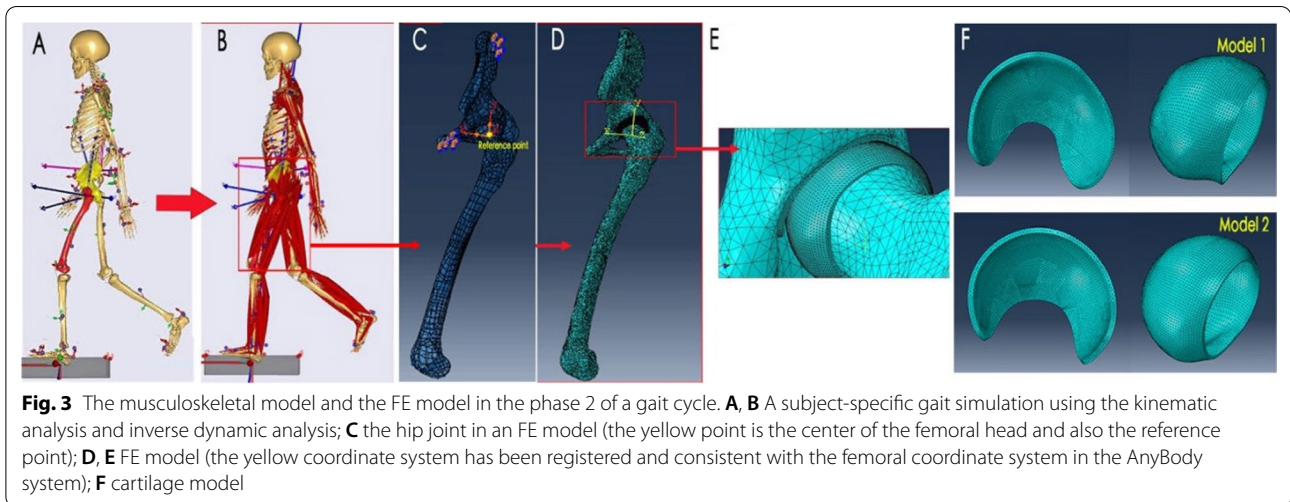


**Fig. 3** The musculoskeletal model and the FE model in the phase 2 of a gait cycle. **A, B** A subject-specific gait simulation using the kinematic analysis and inverse dynamic analysis; **C** the hip joint in an FE model (the yellow point is the center of the femoral head and also the reference point); **D, E** FE model (the yellow coordinate system has been registered and consistent with the femoral coordinate system in the AnyBody system); **F** cartilage model

**Table 1** Properties of materials, the number of elements and elastic modulus in FE models

| Components                      | Element type | Number of elements | Elastic modulus (MPa) | Poisson's ratio |
|---------------------------------|--------------|--------------------|-----------------------|-----------------|
| Cortical bone (femur + ilium)   | C3D10        | Model 1: 22827     | 15,100                | 0.3             |
|                                 |              | Model 2: 19881     |                       |                 |
| Trabecular bone (femur + ilium) | C3D10        | Model 1: 45642     | 445                   | 0.22            |
|                                 |              | Model 2: 41043     |                       |                 |
| Cartilage (femoral head)        | C3D10M       | Model 1: 56783     | 15                    | 0.45            |
|                                 |              | Model 2: 51480     |                       |                 |
| Cartilage (acetabulum)          | C3D10M       | Model 1: 60100     | 15                    | 0.45            |
|                                 |              | Model 2: 56104     |                       |                 |

$$A = \begin{bmatrix} 1 & 0 & 0 \\ 0 & \cos \theta & -\sin \theta_x \\ 0 & \sin \theta & \cos \theta_x \end{bmatrix} \quad (1-1)$$

$$B = \begin{bmatrix} \cos \theta_y & 0 & -\sin \theta_y \\ 0 & 1 & 0 \\ \sin \theta_y & 0 & \cos \theta_y \end{bmatrix} \quad (1-2)$$

$$C = \begin{bmatrix} \cos \theta_z & \sin \theta_z & 0 \\ -\sin \theta_z & \cos \theta_z & 0 \\ 0 & 0 & 1 \end{bmatrix} \quad (1-3)$$

Based on a standard boundary condition described by Phillips et al. [26], encastre was applied at the top of the ilium and pubic areas. The rotation center of the femoral head, obtained using the least-squares spherical fitting method, was selected as the reference node. Nodes on the femoral head surface were constrained by the reference node using a kinematic coupling. The resultant force was applied at the reference point, and the direction of the resultant force at each gait phase was consistent with the reaction force of the hip joint (including the corresponding muscle forces [22] of the hip joint derived from inverse dynamics analysis). The interaction between the femoral head and the acetabulum was simulated by face-to-face contact, and the contact was assumed to be frictionless as it was used in study [27]. The cortical and trabecular bones were set to bind contact.

The mesh sensitivity was performed on a cartilage component rather than the skeletal for contact stress analysis. Since we mainly focus on the contact stress of the hip joint, a finer mesh was used. The maximum contact stress of the femoral head and acetabular was selected for the convergence test (Table 2). Three different mesh sizes were tested on the cartilage models, and the suitability was assessed based on the results of the contact stress analysis (the mesh selection criteria were defined as the changes in contact pressure and area with the difference between the meshes within

1%). According to the results, 1 mm size is selected to divide the cartilage.

**Results**

**Muscle force patterns**

After kinematics optimization, the AnyBody musculo-skeletal models successfully completed gait trials containing complete gait cycles. Data of a single gait cycle (total time of a gait cycle: men: 1.17 s, women: 1.31 s) of the left foot were used for the inverse dynamic analysis. The simulated muscle force patterns in each gait phase during a normal gait cycle were basically consistent with the predicted results which have been reported in similar study [28]. The gluteus maximus, gluteus medius, biceps femoris, quadriceps femoris and adductor magnus showed peak muscle forces at the initial contact phase, while the short external rotator muscles consisting of the gluteus minimus, iliopsoas and adductor longus showed peak muscle forces at the end of the terminal stance phase (Fig. 4). The hip joint reaction force reached a maximum value of 2.9%BM at the end of the terminal stance phase. Twin peaks appeared at the initial contact phase and the end of the terminal stance phase, respectively. The change trend of ground reaction forces was roughly the same as that of Hip joint reaction forces (Fig. 5).

**Contact mechanics of the hip joint**

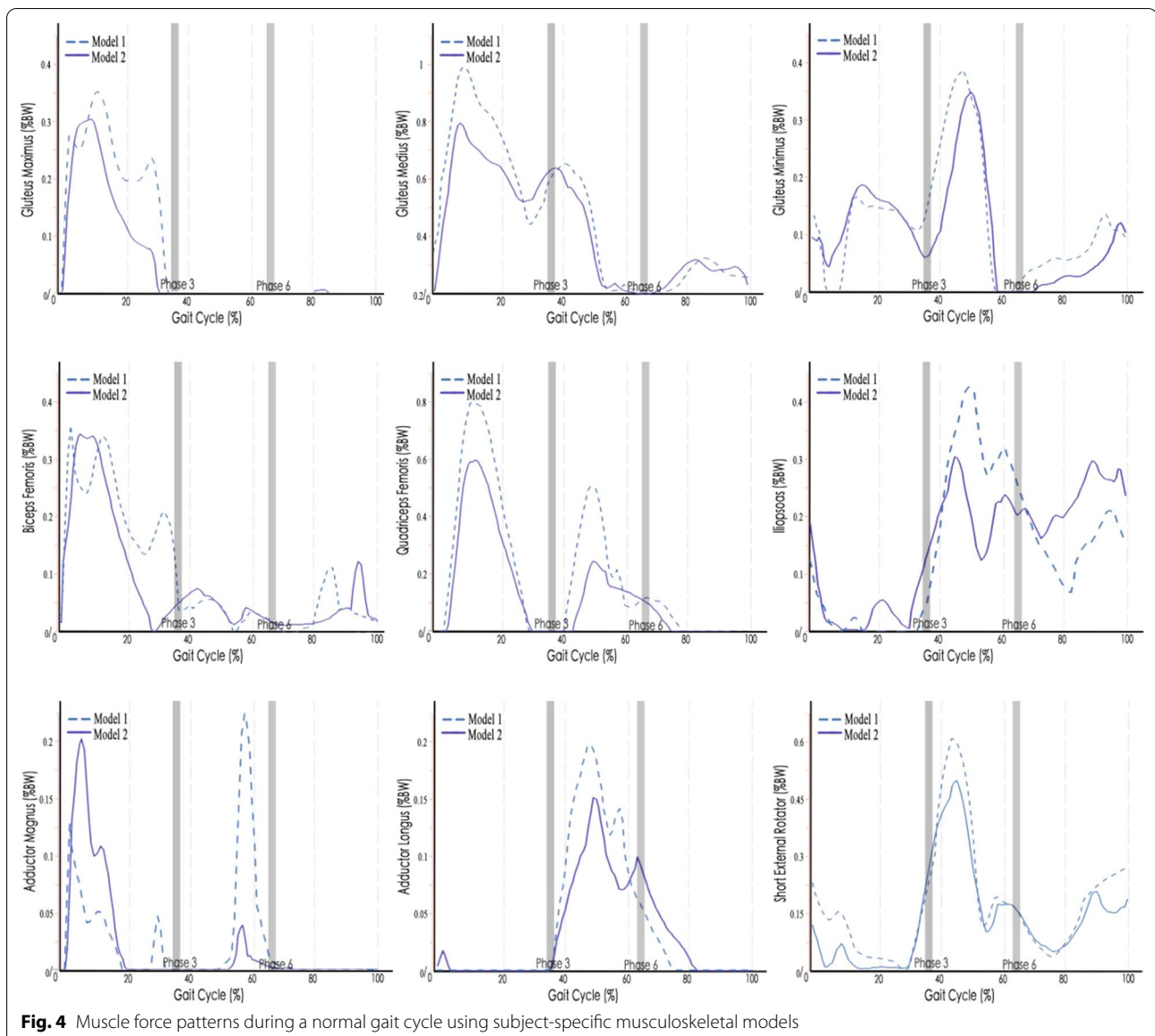
The contact stress distribution of the hip joint during each phase of a normal gait cycle was analyzed by FEA. The results showed that the contact stress at each phase was consistent with the reaction forces of the hip joint. The FEA results showed the time-phase change characteristics of the contact stress distribution of the acetabulum. A peak contact pressure appeared at the loading response phase and the end of the terminal stance phase, during which the maximum contact stress reached 6.91 MPa in model 1 and 6.92 MPa in model 2 (Table 3). These results confirmed previous findings [29]. During a complete gait cycle, the contact pressure was mainly distributed at the top of the femoral head and the dome of the acetabulum, and moved from the anterior column to the posterior column of the acetabulum from phase 1 to phase 8 (Fig. 6). The contact areas were between 316.7 and 787.6 mm<sup>2</sup> in model 1, 293.8 and 998.4 mm<sup>2</sup> in model 2. Model 1 reached a maximum of 787.6mm<sup>2</sup> at the mid-stance phase while model 2 reached a peak of 998.4 mm<sup>2</sup> at the loading response phase.

**Discussion**

In this study, volunteers' gait data were collected, and afterwards a musculoskeletal model was created and a reverse dynamic analysis was performed. We used the results of the inverse dynamic analysis as the boundary

**Table 2** Convergence test for FEA models

| Parameter  | Type 1  | Type 2  | Type 3 |
|--|---------|---------|--------|
| Mesh size (mm)   | 0.5     | 1       | 1.5    |
| Number of meshes (femoral head and acetabular cartilage) | 146,866 | 116,883 | 87,689 |
| Maximum contact stress (MPa)                             | 5.97    | 6       | 6.11   |
| Stress variation rate (%)                                | 0       | 0.5     | 1.8    |
| Contact area (mm <sup>2</sup> )                          | 780.8   | 787.6   | 783.1  |
| Contact area variation rate (%)                          | 0       | 0.8     | 0.5    |



and load settings of the FE model of the hip joint. FEA was used to analyze the contact stress of the hip joint at each phase in a complete gait cycle. This study confirmed that the hip joint reaction was constantly changing during a complete gait cycle. Moreover, the contact stresses were the highest at the terminal stance phase at both models. Double peaks occurred at the loading response phase and at the end of the terminal stance phase, but not in the mid-stance phase.

Moreover, most of previous studies about contact mechanics of legs using the FE model were based on a standing position [6, 30–32], which could simplify the analysis and could not objectively reflect dynamic stress distribution. Therefore, it was easy to underestimate

the damages of the contact stresses, while the relevant results could not truly reflect the human body. Studies have shown that excessive stress on the hip joint was the main cause of hip osteoarthritis [33, 34], which also reminds us that patients with clinical hip osteoarthritis are more prone to worsening in these two periods. Contact stress and maximum shear stress could be used to predict the fissuring of acetabular cartilage, which is one of the early symptoms of hip osteoarthritis in the body [35, 36]. The cross-cartilage changes of contact stress are related to the formation of larger shear forces [37]. Our study confirmed that the intensity and distribution area of contact stress changed with gait, which may damage articular cartilage and cause hip

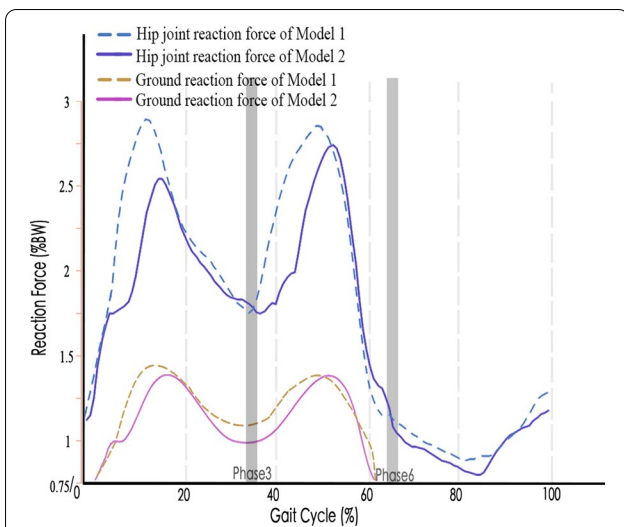


**Fig. 5** Hip joint reaction forces and ground reaction forces for subject-specific musculoskeletal models during gait cycle

anterolateral part of the top of the femoral head, moving from the anterior column to the posterior column of the acetabulum during a gait cycle. Therefore, in the daily diagnosis and treatment of femoral head necrosis, we must focus on the anterolateral part of the top of the femoral head to predict an early-on collapse, as this area bears the most concentrated forces at the early stage. This result is also helpful for guiding the daily rehabilitation exercise of patients with femoral head necrosis and for providing valuable recommendations for the selection of treatment regimens.

Few studies have analyzed changes in the dynamic contact stress distribution during a gait cycle. Brown et al. [38] implanted a resistive sensor on the surface of the acetabular cartilage in vivo to monitor the surface mechanics. The results obtained by this method, though relatively reliable, are highly invasive, technically demanding and cost-consuming. Wang et al. [39] analyzed the stress distribution during a normal gait cycle using the FEA and concluded that in a complete gait acetabulum contact stress presented bimodal distribution while the peak appeared in the starting phase and the support phase, respectively, with the maximum

osteoarthritis. Other findings of our study were that the acetabular contact stress was mainly distributed in the medial part of the dome of the acetabulum and the

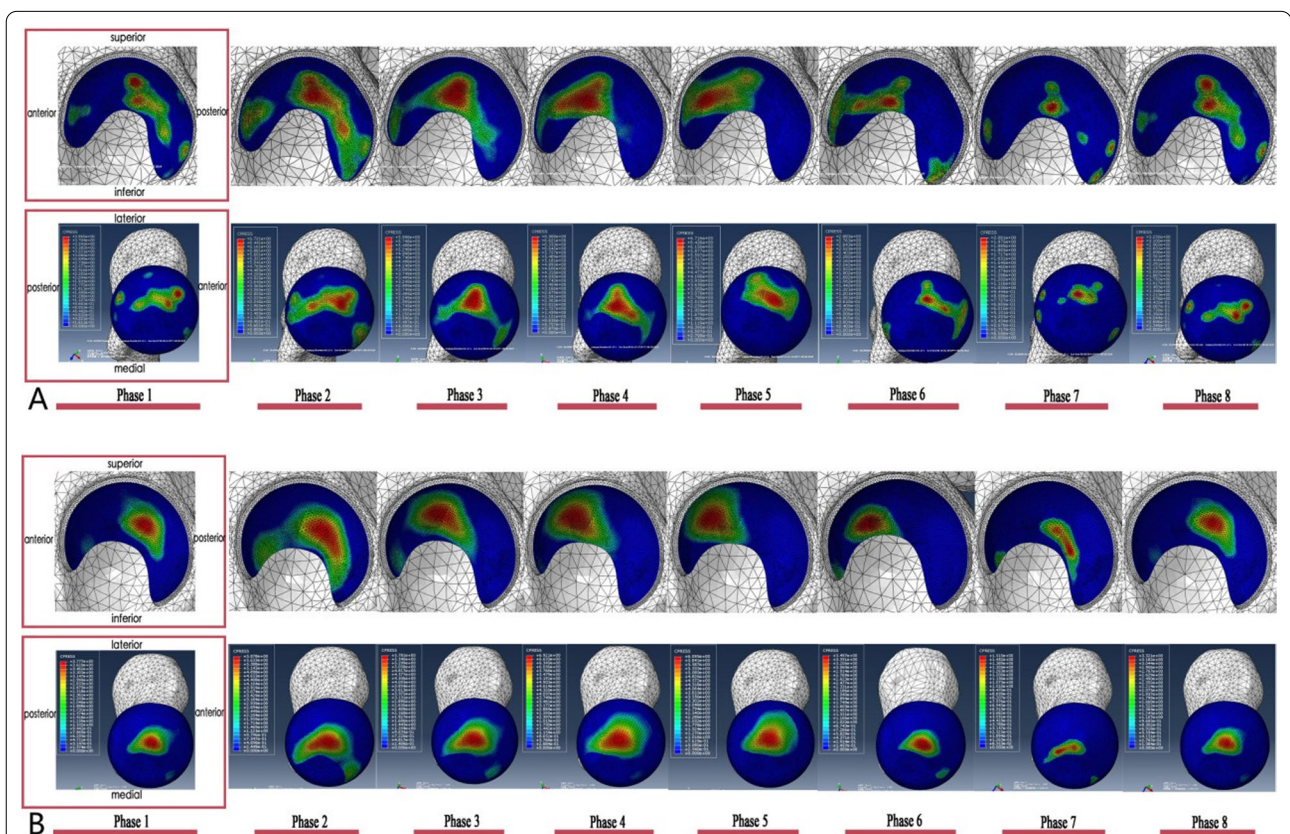


**Fig. 6** The nephograms of the contact pressure (CPRESS) on the acetabulum and femoral head cartilage surface during each phase of a gait cycle. **A** Model 1, **B** Model 2



**Table 3** Hip joint reaction forces, peak contact pressure and contact area changes during different phases of a gait cycle

| Phases of a gait cycle | Components ( $F_x$ , $F_y$ , $F_z$ ) of hip joint reaction forces (N) |         |        |         |         |        | Peak contact pressure (MPa) |         | Contact area (mm <sup>2</sup> ) |         |
|------------------------|---|---------|--------|---------|---------|--------|-----------------------------|---------|---------------------------------|---------|
|                        | Model 1   |         |        | Model 2 |         |        | Model 1                     | Model 2 | Model 1                         | Model 2 |
|                        | $-F_x$  | $-F_y$  | $-F_z$ | $-F_x$  | $-F_y$  | $-F_z$ |                             |         |                                 |         |
| 1                      | 89.32   | 746.57  | 171.35 | 29.23   | 737.69  | 182.3  | 3.87                        | 3.78    | 607.2                           | 548.3   |
| 2                      | 517.5   | 1706.6  | 636.6  | 241.27  | 1472.22 | 300.8  | 6.72                        | 5.88    | 720.4                           | 998.4   |
| 3                      | 151.03  | 1211.7  | 404.1  | 103.97  | 1053.17 | 222.22 | 6                           | 5.78    | 787.6                           | 717.4   |
| 4                      | -6  | 1562.5  | 442.43 | 67      | 1372.2  | 377.38 | 6.91                        | 6.92    | 758.1                           | 943.2   |
| 5                      | -34.15  | 1837.55 | 342.37 | 11.67   | 1622.1  | 178.21 | 6.72                        | 6.1     | 721.1                           | 912.2   |
| 6                      | 172.64  | 932.92  | 237.38 | 231.22  | 1033.38 | 334.17 | 2.88                        | 3.5     | 589.3                           | 672.2   |
| 7                      | 91.23   | 478.7   | 243.72 | 45.22   | 344.83  | 177.31 | 2.06                        | 1.52    | 316.7                           | 238.8   |
| 8                      | 92.67   | 717.3   | 172.74 | 37.18   | 710.26  | 177.9  | 3.24                        | 3.32    | 586.4                           | 426.1   |

Force components ( $F_x$ ,  $F_y$ ,  $F_z$ ) corresponded to the local coordinate system of the thigh in MS models,  $F_x$ : medio-lateral,  $F_y$ : vertical,  $F_z$ : anterior-posterior. Peak contact pressure and contact area were detected using the FE analysis

stress ranging from 4.2 to 3.3 MPa. Moreover, the acetabulum contact area reached the maximum of 1470 mm<sup>2</sup>, in the initial phase. Anderson et al. [40] showed that the maximum contact stress of the acetabulum during a walking gait was 10.78 MPa. After the FE analysis of 10 healthy volunteers, Michael D. Harris et al. [41] believed that the acetabular contact stress reached its peak ( $7.52 \pm 2.11$  mpa) when walking on the heel, while the average contact area occupied 34% of the total acetabular area. A study by Wu et al. [42] reported that in a gait cycle the maximum contact pressure reached 7.48 MPa. Their results are inconsistent with other studies which can be explained by their failure to consider impacts from the surrounding soft tissues such as muscles and ligaments. Besides, there are still differences between simulated data and gait trajectories of subjects. Li's [43] study uses the same to use the MS and FEA as this study for coupling modeling. The results showed that the maximum contact stress of the hip joint is 6.5 MPa presented to the initial contact phase, which is close to the results of this study. However, the used gait data were taken from public databases, not from the same researcher, and therefore it failed to achieve personalized research. Our research uses the "gait-MS-FE" method to add muscle strength around the joints to the model, which also reduces the influence of gait differences between individuals on the results of the study, so the results of this study are more credible.

The innovation of our research lies the fact that the method of "gait-MS-FE" is applied to the study of hip joint mechanics, and to personally study the changes in the contact stress of the hip joint during a gait cycle. This method can also be applied to the research of the contact stress changes of the hip in special positions and the contact stress of certain hip diseases. Genda et al.

[44] analyzed and compared the contact stress between 112 healthy individuals and 66 patients, and the results showed that the contact stress in the normal acetabulum can be evenly distributed on the surface of the joints. Moreover, the articular contact stress in patients with joint dysplasia relatively concentrated on the anterior lateral edges of the acetabulum. However, the study only studied the contact stress in a stationary state and failed to pay attention to the characteristics of the entire gait. Robert et al. [45] studied the changes of the acetabular contact stress in 12 patients who had undergone periacetabular rotational osteotomy for nearly 10 years, which had a clinical implication for the treatment of hip dysplasia. However, the dynamic analysis of the whole gait process was ignored and the effect of the surrounding muscle force on the results was not considered. If the "gait-MS-FE" method is applied to the research of these diseases, it could make the research results more credible.

However, limitations in this study must be acknowledged. Like most studies about the FEA [46–49], all bone models were assigned with homogenization, while the actual bone density of different parts is uneven. The cartilage thickness of models was universal. In these regards, the reliability of our results may be reduced. Moreover, this study failed to consider the muscle forces on other joints such as the knee joint and the other leg, which may also have an impact on the contact stress of the hip joint. The influence of labrum in the contact stress of the hip joint has also been neglected. We utilized fixed boundary conditions at the top of the ilium and pubic area, while the fixed model is not representative of the in vivo environment. In the follow-up research, we will build the model more finely. In addition, this study failed to consider the influence of different walking speeds on the contact stress of the hip joint, Hu et al. [50] found that

changes in walking speed may lead to changes in joint mechanics. We could explore the influence of different walking speeds on the contact stress of the hip joint in future researches. In this study, the result of maximum stress of 2 people with different BMI was too similar. So it cannot be ruled out whether BMI has an impact on the experimental results. In the future, a larger sample of research could be carried out.

## Conclusions

To sum up, the subject-specific gait in combination with an inverse dynamic analysis of the MS provides pre-processing parameters for FE simulation for biomechanical analysis of hip joint. In this study, the contact stress of the hip joint in a gait cycle was studied by constructing the “gait-MS-FE” method.

## Abbreviations

MS: Musculoskeletal system; FE: Finite element; BW: Body weight; FEA: Finite element analysis.

## Acknowledgements

Not applicable.

## Author contributions

XBL was responsible for the design and implementation of the study presented. YP and LTY were responsible for the development of the finite element models. LTY and XJL conducted the experiments and were responsible for the acquisition of the data. ZQZ and LQZ were responsible for recruiting volunteers. GYL and LCR provided technical support for gait analysis (BTS Bioengineering, Italy). XBL prepared the initial draft of the manuscript. ZQW, WQS and HW gave critical feedback during the study and critically revised the submitted manuscript for important intellectual content. All authors have read and approved the final manuscript to be submitted.

## Funding

The authors acknowledge the Natural Science Foundation of China (Grant No. 81873327), Natural Science Foundation of Guangdong (Grant No. 2015A030313353), Scientific Research Project of Chinese Medicine of Guangdong (Grant No. 20191116) and Excellent Doctoral Dissertation Incubation Grant of First Clinical School of Guangzhou University of Chinese Medicine (Grant No. YB201802).

## Availability of data and materials

Not applicable.

## Declarations

### Ethics approval and consent to participate

All procedures of this study were in accordance with the ethical standards laid down in the 2013 Declaration of Helsinki and approved by the Ethics Committee of the First Affiliated Hospital of Guangzhou University of Chinese Medicine (No. K [2019]124).

### Consent for publication

Not applicable.

### Competing interests

The authors declare that they have no competing interests.

### Author details

<sup>1</sup>The First Clinical Medical College, Guangzhou University of Chinese Medicine, Guangzhou 510405, Guangdong, China. <sup>2</sup>The Lab of Orthopaedics of Chinese

Medicine of Lingnan Medical Research Center, Guangzhou University of Chinese Medicine, Guangzhou 510405, Guangdong, China. <sup>3</sup>Department of Joint Orthopaedic, the First Affiliated Hospital, Guangzhou University of Chinese Medicine, Guangzhou 510405, Guangdong, China. <sup>4</sup>Guangzhou University, Guangzhou 510006, Guangdong, China. <sup>5</sup>Brain Hospital Affiliated to Jinan University, Guangzhou 510510, Guangdong, China. <sup>6</sup>The Third Affiliated Hospital, Guangzhou University of Chinese Medicine, Guangzhou 510240, Guangdong, China. <sup>7</sup>Present Address: Second People's Hospital of Shenzhen, Shenzhen 518000, Guangdong, China.

Received: 16 October 2021 Accepted: 20 March 2022

Published online: 14 May 2022

## References

- Quinn RH, Murray J, Pezold R, Hall Q. Management of osteoarthritis of the hip. *J Am Acad Orthop Surg*. 2018;26(20):e434–6.
- Stief F, Schmidt A, van Drongelen S, Lenarz K, Froemel D, Tarhan T, Lutz F, Meurer A. Abnormal loading of the hip and knee joints in unilateral hip osteoarthritis persists two years after total hip replacement. *J Orthop Res*. 2018. <https://doi.org/10.1002/jor.23886> (published online ahead of print).
- Warashina H, Kato M, Kitamura S, Kusano T, Hasegawa Y. The progression of osteoarthritis of the hip increases degenerative lumbar spondylolisthesis and causes the change of spinopelvic alignment. *J Orthop*. 2019;16(4):275–9.
- Nho SJ, Kymes SM, Callaghan JJ, Felson DT. The burden of hip osteoarthritis in the United States: epidemiologic and economic considerations. *J Am Acad Orthop Surg*. 2013;21(Suppl 1):S1–6.
- Koenig L, Zhang Q, Austin MS, Demiralp B, Fehring TK, Feng C, Mather RC, Nguyen JT, Saavoss A, Springer BD Jr, Yates AJ. Estimating the societal benefits of THA after accounting for work status and productivity: a Markov model approach. *Clin Orthop Relat Res*. 2016;474(12):2645–54.
- Kitamura K, Fujii M, Utsunomiya T, Iwamoto M, Ikemura S, Hamai S, Motomura G, Todo M, Nakashima Y. Effect of sagittal pelvic tilt on joint stress distribution in hip dysplasia: A finite element analysis. *Clin Biomech (Bristol, Avon)*. 2020;74:34–41.
- Liu L, Siebenrock K, Nolte LP, Zheng G. Biomechanical optimization-based planning of periacetabular osteotomy. *Adv Exp Med Biol*. 2018;1093:157–68.
- Polkowski GG, Clohisy JC. Hip biomechanics. *Sports Med Arthrosc Rev*. 2010;18(2):56–62.
- Wootten ME, Kadaba MP, Cochran GV. Dynamic electromyography. II. Normal patterns during gait. *J Orthop Res*. 1990;8(2):259–65.
- Vogel D, Wehmeyer M, Keibach M, Heyer H, Bader R. Stress and strain distribution in femoral heads for hip resurfacing arthroplasty with different materials: a finite element analysis. *J Mech Behav Biomed Mater*. 2021;113:104115.
- Xu J, Zhan S, Ling M, Jiang D, Hu H, Sheng J, Zhang C. Biomechanical analysis of fibular graft techniques for nontraumatic osteonecrosis of the femoral head: a finite element analysis. *J Orthop Surg Res*. 2020;15(1):335.
- Akrami M, Craig K, Dibaj M, Javadi AA, Benattayallah A. A three-dimensional finite element analysis of the human hip. *J Med Eng Technol*. 2018;42(7):546–52.
- Todd JN, Maak TG, Anderson AE, Ateshian GA, Weiss JA. How does chondrolabral damage and labral repair influence the mechanics of the hip in the setting of cam morphology? A finite-element modeling study. *Clin Orthop Relat Res*. 2021;480(3):602–15.
- Li M, Venäläinen MS, Chandra SS, Patel R, Fripp J, Engstrom C, Korhonen RK, Töyräs J, Crozier S. Discrete element and finite element methods provide similar estimations for hip joint contact mechanics during walking gait. *J Biomech*. 2021;115:110163.
- Yoshida H, Faust A, Wilckens J, Kitagawa M, Fetto J, Chao EY. Three-dimensional dynamic hip contact area and pressure distribution during activities of daily living. *J Biomech*. 2006;39(11):1996–2004.
- Russell ME, Shivanna KH, Grosland NM, Pedersen DR. Cartilage contact pressure elevations in dysplastic hips: a chronic overload model. *J Orthop Surg Res*. 2006;1:6.

17. Chegini S, Beck M, Ferguson SJ. The effects of impingement and dysplasia on stress distributions in the hip joint during sitting and walking: a finite element analysis. *J Orthop Res*. 2009;27(2):195–201.
18. Henak CR, Abraham CL, Anderson AE, Maas SA, Ellis BJ, Peters CL, Weiss JA. Patient-specific analysis of cartilage and labrum mechanics in human hips with acetabular dysplasia. *Osteoarthr Cartil*. 2014;22(2):210–7.
19. Hellwig FL, Tong J, Hussell JG. Hip joint degeneration due to cam impingement: a finite element analysis. *Comput Methods Biomech Biomed Engin*. 2016;19(1):41–8.
20. Ng KC, Mantovani G, Lamontagne M, Labrosse MR, Beaulé PE. Increased hip stresses resulting from a cam deformity and decreased femoral neck-shaft angle during level walking. *Clin Orthop Relat Res*. 2017;475(4):998–1008.
21. Anderson AE, Ellis BJ, Maas SA, Weiss JA. Effects of idealized joint geometry on finite element predictions of cartilage contact stresses in the hip. *J Biomech*. 2010;43(7):1351–7.
22. Damsgaard M, Rasmussen J, Christensen ST. Analysis of musculoskeletal systems in the AnyBody Modeling System. *Simul Model Pract Theory*. 2006;14(8):1100–11.
23. Niknafs N, Murphy RJ, Armiger RS, Lepistö J, Armand M. Biomechanical factors in planning of periacetabular osteotomy. *Front Bioeng Biotechnol*. 2013;10(1):20.
24. Zou Z, Chávez-Arreola A, Mandal P, Board TN, Alonso-Rasgado T. Optimization of the position of the acetabulum in a ganz periacetabular osteotomy by finite element analysis. *J Orthop Res*. 2013;31(3):472–9.
25. Kharb A, Saini V, Jain YK. A review of gait cycle and its parameters. *IJCEM Int J Comput Eng Manag*. 2011;13:78–83.
26. Phillips AT, Pankaj P, Howie CR, Usmani AS, Simpson AH. Finite element modelling of the pelvis: inclusion of muscular and ligamentous boundary conditions. *Med Eng Phys*. 2007;29(7):739–48.
27. Caligaris M, Ateshian GA. Effects of sustained interstitial fluid pressurization under migrating contact area, and boundary lubrication by synovial fluid, on cartilage friction. *Osteoarthr Cartil*. 2008;16(10):1220–7.
28. Bergmann G, Deuretzbacher G, Heller M, Graichen F, Rohlmann A, Strauss J, Duda GN. Hip contact forces and gait patterns from routine activities. *J Biomech*. 2001;34(7):859–71.
29. Krebs DE, Robbins CE, Lavine L, Mann RW. Hip biomechanics during gait. *J Orthop Sports Phys Ther*. 1998;28(1):51–9.
30. Luo C, Wu XD, Wan Y, Liao J, Cheng Q, Tian M, Bai Z, Huang W. Femoral stress changes after total hip arthroplasty with the ribbed prosthesis: a finite element analysis. *Biomed Res Int*. 2020;2020:6783936.
31. Shankar S, Nithyaprakash R, Santhosh BR, Uddin MS, Pramanik A. Finite element submodeling technique to analyze the contact pressure and wear of hard bearing couples in hip prosthesis. *Comput Methods Biomech Biomed Engin*. 2020;23(8):422–31.
32. Abdullah AH, Todo M, Nakashima Y. Prediction of damage formation in hip arthroplasties by finite element analysis using computed tomography images. *Med Eng Phys*. 2017;44:8–15. <https://doi.org/10.1016/j.medengphy.2017.03.006>.
33. Genda E, Iwasaki N, Li G, MacWilliams BA, Barrance PJ, Chao EY. Normal hip joint contact pressure distribution in single-leg standing—effect of gender and anatomic parameters. *J Biomech*. 2001;34(7):895–905.
34. Mavric B, Pompe B, Antolic V, Daniel M, Iglic A, Kralj-Iglic V. Mathematical estimation of stress distribution in normal and dysplastic human hips. *J Orthop Res*. 2002;20(5):1025–30.
35. Atkinson TS, Haut RC, Altiero NJ. Impact-induced fissuring of articular cartilage: an investigation of failure criteria. *J Biomech Eng*. 1998;120(2):181–7.
36. Haut RC, Ide TM, De Camp CE. Mechanical responses of the rabbit patello-femoral joint to blunt impact. *J Biomech Eng*. 1995;117(4):402–8.
37. Henak CR, Ateshian GA, Weiss JA. Finite element prediction of transchondral stress and strain in the human hip. *J Biomech Eng*. 2014;136(2):021021.
38. Brown TD, Shaw DT. In vitro contact stress distributions in the natural human hip. *J Biomech*. 1983;16(6):373–84.
39. Wang G, Huang W, Song Q, Liang J. Three-dimensional finite analysis of acetabular contact pressure and contact area during normal walking. *Asian J Surg*. 2017;40(6):463–9.
40. Anderson AE, Ellis BJ, Maas SA, Peters CL, Weiss JA. Validation of finite element predictions of cartilage contact pressure in the human hip joint. *J Biomech Eng*. 2008;130(5):051008.
41. Harris MD, Anderson AE, Henak CR, Ellis BJ, Peters CL, Weiss JA. Finite element prediction of cartilage contact stresses in normal human hips. *J Orthop Res*. 2012;30(7):1133–9.
42. Hui-Hui Wu, Wang D, Ma A-B, Dong-Yun Gu. Hip joint geometry effects on cartilage contact stresses during a gait cycle. *Conf Proc IEEE Eng Med Biol Soc*. 2016;2016:6038–41.
43. Li J. Development and validation of a finite-element musculoskeletal model incorporating a deformable contact model of the hip joint during gait. *J Mech Behav Biomed Mater*. 2021;113:104136.
44. Genda E, Konishi N, Hasegawa Y, Miura T. A computer simulation study of normal and abnormal hip joint contact pressure. *Arch Orthop Trauma Surg*. 1995;114(4):202–6.
45. Armiger RS, Armand M, Talloth K, Lepistö J, Mears SC. Three-dimensional mechanical evaluation of joint contact pressure in 12 periacetabular osteotomy patients with 10-year follow-up. *Acta Orthop*. 2009;80(2):155–61.
46. Mukherjee K, Gupta S. The effects of musculoskeletal loading regimes on numerical evaluations of acetabular component. *Proc Inst Mech Eng H*. 2016;230(10):918–29.
47. Fernandez J, Sartori M, Lloyd D, Munro J, Shim V. Bone remodelling in the natural acetabulum is influenced by muscle force-induced bone stress. *Int J Numer Method Biomed Eng*. 2014;30(1):28–41.
48. Hua X, Li J, Jin Z, Fisher J. The contact mechanics and occurrence of edge loading in modular metal-on-polyethylene total hip replacement during daily activities. *Med Eng Phys*. 2016;38(6):518–25.
49. Dikko Kaze A, Maas S, Arnoux PJ, Wolf C, Pape D. A finite element model of the lower limb during stance phase of gait cycle including the muscle forces. *Biomed Eng Online*. 2017;16(1):138.
50. Hu Z, Ren L, Hu D, Gao Y, Wei G, Qian Z, Wang K. Speed-related energy flow and joint function change during human walking. *Front Bioeng Biotechnol*. 2021;9:666428.

## Publisher's Note

Springer Nature remains neutral with regard to jurisdictional claims in published maps and institutional affiliations.

**Ready to submit your research? Choose BMC and benefit from:**

- fast, convenient online submission
- thorough peer review by experienced researchers in your field
- rapid publication on acceptance
- support for research data, including large and complex data types
- gold Open Access which fosters wider collaboration and increased citations
- maximum visibility for your research: over 100M website views per year

**At BMC, research is always in progress.**

Learn more [biomedcentral.com/submissions](https://biomedcentral.com/submissions)

